Since January 2020 Elsevier has created a COVID-19 resource centre with free information in English and Mandarin on the novel coronavirus COVID-19. The COVID-19 resource centre is hosted on Elsevier Connect, the company's public news and information website.

Biosensors and Bioelectronics 165 (2020) 112363

Contents lists available at ScienceDirect

Biosensors and Bioelectronics

journal homepage: http://www.elsevier.com/locate/bios

Graphene field-effect transistor biosensor for detection of biotin with ultrahigh sensitivity and specificity

Shiyu Wang [a,**], Md Zakir Hossain [b,*], Kazuo Shinozuka [c], Natsuhiko Shimizu [b], Shunya Kitada [b], Takaaki Suzuki [d], Ryo Ichige [d], Anna Kuwana [a], Haruo Kobayashi [a,***]

[a] Division of Electronics and Informatics, Graduate School of Science and Engineering, Gunma University 1-5-1 Tenjin-cho, Kiryu, 376-8515, Japan
[b] Gunma University Initiative for Advanced Research (GIAR), Gunma University, Japan
[c] Division of Molecular Science, Graduate School of Science and Technology, Gunma University, Japan
[d] Division of Mechanical Science and Technology, Gunma University, Kiryu, 376-8515, Japan

ARTICLE INFO

Keywords:
Graphene
Field-effect transistor
Biosensor
Avidin
Biotin
Clinical diagnosis

ABSTRACT

Because avidin and biotin molecules exhibit the most specific and strongest non-covalent interaction, avidin-biotin technology is widely used in ELISA (enzyme-linked immunosorbent assay) kits for the detection of different bio-macromolecules linked to different diseases including cancer and influenza. Combining the outstanding electrical conductivity (200,000 $cm^2V^{-1}s^{-1}$) of graphene with the unique avidin and biotin interaction, we demonstrate a novel graphene field-effect transistor (GFET) biosensor for the quantitative detection of bio-macromolecules. The GFET consists of six pairs of interdigital Cr/Au electrodes supported on Si/SiO_2 substrate with an avidin immobilized single layer graphene channel as the sensing platform. By monitoring the real time current change upon the addition of biotin solution in bovine serum albumin (BSA) in the silicone pool preformed onto the GFET, the lowest detectable biotin concentration is estimated to be 90 fg/ml (0.37 pM). The specificity of the GFET is confirmed both by controlled and real sample measurements. From the magnitude of current change upon the addition of different concentrations of biotin solutions, the dissociation constant K_d is estimated to be 1.6×10^{-11} M. Since biotin is capable of conjugating with proteins, nucleotides and other bio-macromolecules without altering their properties, the present GFET sensor with its ultra-high sensitivity (0.37 pM) and specificity can be tailored to the rapid point-of-care detection of different types of desired biomolecules at very low concentration level through biotinylation as well as the exogenous biotin in blood serum.

1. Introduction

The strong interaction between avidin and biotin has been widely exploited in many applications such as protein and nucleic acid detection, immobilization, and purification methods (Guesdon et al., 1979; Hsu et al., 1981a, 1981b). Avidin is a tetrameric biotin-binding protein produced in the oviducts of birds, reptiles, and amphibians and is deposited in the whites of their eggs. Dimeric members of the avidin family are also found in some bacteria (Helppolainen et al., 2007). In chicken egg white, avidin makes up approximately 0.05% of total protein (approximately 1800 μg per egg). The tetrameric protein contains four identical subunits (homotetramer), each of which can bind to biotin (vitamin B7, vitamin H) with a high degree of affinity and specificity (Green, 1963). Biotin is involved in a wide range of metabolic processes, both in humans and other organisms, primarily related to the utilization of fats, carbohydrates, and amino acids (Zempleni et al., 2009). Because of its small size, biotin is a useful label for many proteins and nucleotides as it does not change the original properties of the proteins or nucleotides. The process of labeling a protein or nucleotide with biotin is known as biotinylation. It is also important that biotin protein ligases can attach biotin to specific lysine residues in vitro or in living cells (Chivers et al., 2011). The interaction between avidin and biotin is known to be the most specific and strongest non-covalent interaction ($Kd = 10^{-15}$ M) between a protein and ligand (Green, 1963; Morag et al., 1996). The exceptionally strong affinity of avidin for biotin arises from the hydrophobic interactions of biotin and aromatic amino acids

* Corresponding author.
** Corresponding author.
*** Corresponding author.
E-mail addresses: t182d001@gunma-u.ac.jp (S. Wang), zakir@gunma-u.ac.jp (M.Z. Hossain), koba@gunma-u.ac.jp (H. Kobayashi).

https://doi.org/10.1016/j.bios.2020.112363
Received 14 April 2020; Received in revised form 28 May 2020; Accepted 3 June 2020
Available online 4 June 2020

arranged in the binding pocket of avidin and multiple hydrogen bonding between heteroatoms in the ureido ring of biotin and asparagine, serine, tyrosine, and threonine residues in avidin (Chivers et al., 2011). Due to the strong interaction, the avidin-biotin complex is robust and stable against temperature, pH, harsh organic solvents and denaturing reagents. Given the unique properties of the avidin-biotin system, it is used often in enzyme-linked immunosorbent assay (ELISA) for many different types of medical applications such as cancer diagnosis (Ben Aissa et al., 2017; Gutiérrez-Zúñiga and Hernández-López, 2016; Lakshmipriya et al., 2016; Yang and Tseng, 2016). In addition, the avidin-biotin system is also used in other exciting applications such as labeled immunosensors (Yang et al., 2010), polymer-based detection (Ballesta-Claver et al., 2012).

To date, ELISA is one of the most widely used techniques for the detection of various types of biomarkers linked to various diseases such as influenza, cancer, AIDS (Carinelli et al., 2016; Safaei et al., 2015; Tauriello et al., 2018). Indeed, the detection of biomarkers by ELISA is based on the optical measurement of fluorescent markers, which requires integrated use of advanced spectral equipment. Biotinylated antibody and streptavidin-conjugated horseradish peroxide (streptavidin-HRP) often are used with ELISA to enhance the detection of various kinds of targets (Agnolon et al., 2020). A large range of clinical screening applications including those for infectious diseases such as SARS-CoV-2 (Wang et al., 2020) can be performed using ELISA diagnostic kits. However, from the sample collection to results output, the whole ELISA detection process takes at least a few hours and requires a specific analyzer (Rubio et al., 2017; Safaei et al., 2015). Moreover, because of the sensitivity of the ELISA kits, it cannot be used for the early stage diagnosis of a disease such as cancer (Fiala and Diamandis, 2018). Hence, the conventional ELISA kits cannot cope with urgent, quick and vigorous testing demands such as the recent COVID-19 pandemic. Fortunately, the graphene based FET sensor appears as a most promising approach to point-of-care medical diagnostics for rapid, sensitive, specific, low-cost detection and quantification of biomarkers (Afsahi et al., 2018), and thereby could be a complementary diagnostic tool to ELISA kits.

Graphene is a single atom thick, sp^2-hybridized two-dimensional carbon material. Since its discovery, graphene's unique and extreme properties has triggered some revolutionary applications, such as batteries and super capacitor (Hu et al., 2016; Wen et al., 2016; Xiao et al., 2017; Zhang et al., 2018). Graphene also holds promise for energy storage (Yang et al., 2013), nano energy (Wu et al., 2012), catalysis (Machado and Serp, 2012), coating (Singh Raman et al., 2012) and biomedicine (Yang et al., 2012). Because of its extremely high electrical conductivity (200,000 $cm^2V^{-1}s^{-1}$) and ambipolar transfer characteristics (Geim and Novoselov, 2009; Novoselov et al., 2004), graphene is considered as the most promising material for different types of ultra-sensitive graphene field-effect transistor (GFET) sensors such as chemical and biosensor. The extreme sensitivity of GFET relates to the Fermi energy shift induced by the adsorption of any molecules involving charge transfer between substrate and molecules, which ultimately changes the conductivity of graphene (Alberto and Pier, 2020). Even without any traceable change of Fermi level, any localized orbital distortion induced by the adsorbed molecule can also change the conductivity of graphene (Alberto and Pier, 2020). Hence, the carrier density of graphene is expected to be altered even by the non-covalent binding of biomolecules onto the surface, i.e., the electrical conductivity of graphene is expected to be altered by the non-covalent binding of a very small concentration of biomolecules onto the graphene surface.

The field-effect transistor (FET) is a type of transistor that uses an electric field to control the flow of current. In a typical FET, there are three terminals: source, gate, and drain. The flow of current between the drain and source through the conducting channel is controlled by the gate voltage (Frank, 2010). For the GFET sensor, not only the external gate voltage can regulate the current, but any change in graphene electronic states caused by the adsorption of molecules can also regulate the source-drain current (Deana et al., 2019). Note that graphene act as the conducting channel between source and drain in GFET. Thus, when a molecule is adsorbed onto the graphene surface in a working FET, the electronic states of the graphene channel are changed, and thereby changes the source-drain current. Hence the binding of any molecules onto the graphene channel of the GFET will trigger a real time change in source-drain current. Thus, the standard current vs concentration curve permits the quantitative analysis of target molecules. To date, a number of studies have been reported on the potential applications of GFET in biosensors (Ohno et al., 2009, 2010; Matsumoto, 2015; Afsahi et al., 2018; Cai et al., 2015; Pan et al., 2017; Xu et al., 2017; Yang et al., 2017; Yu et al., 2019; Zhou et al., 2017; Deana et al., 2019; Taniguchi et al., 2019; Nozaki et al., 2020). The detection of bio-macromolecules including cancer markers and RNAs by GFET biosensors has been reported using various types of acceptor/receptor design (Afsahi et al., 2018; Cai et al., 2015; Ohno et al., 2010; Pan et al., 2017; Wang et al., 2019; Xu et al., 2017; Yang et al., 2017; Yu et al., 2019; Zhou et al., 2017). Ohno et al. have reported the electrolyte gated GFET for pH and protein detection (Ohno et al., 2009). The aptamer modified GFET has been reported for label free detection of immunoglobulin (IgE) protein (Ohno et al., 2010). Recently, GFET has been shown to detect ethanol in ppb level (Nozaki et al., 2020). Deana et al. have reported the label free sensing of exosomes using functionalized graphene based FET (Deana et al., 2019).

In spite of enormous potential of avidin-biotin technology, the sensitivity and specificity of avidin-biotin interaction has not been investigated with GFET. Recently, Taniguchi et al. have studied the effect of pH on the interaction between avidin and iminobiotin using epitaxial graphene on SiC based FET and emphasized the need for concentration dependent measurements (Taniguchi et al., 2019). Here, we report the development of a novel GFET biosensor consisting of six pairs of interdigital electrodes covered by single layer graphene for detecting biotin molecules with ultrahigh sensitivity and specificity. Real time measurements are realized by monitoring the drain-source current changes upon the entry of biotin solution onto the avidin immobilized graphene channel. The detection limit of biotin is estimated to be 90 fg/ml (0.37 pM). Since the biotin can conjugate with a variety of proteins and nucleotides through biotinylation without changing their original properties, the proposed GFET, which integrates the graphene's extreme electrical conductivity with the unique avidin-biotin technology, is expected to be a breakthrough in the development of GFET biosensors for the rapid and point of care diagnosis of infectious diseases and different biomarkers with ultrahigh sensitivity and specificity.

2. Material and methods

2.1. Materials and instruments

A 4-inch 285 nm SiO_2/Si wafer was purchased from ALLIANCE Biosystems (Osaka, Japan). The chemical vapor deposition (CVD) graphene on copper foil was purchased from Chongqing Graphene Technology Co., Ltd (Chongqing, China). Poly (methyl methacrylate) (PMMA) was purchased from Sigma-Aldrich (Tokyo, Japan). Ammonium peroxodisulfate was purchased from Kanto Chemical Co., Inc. (Tokyo, Japan). PBASE was synthesized. Neutravidin protein and phosphate-buffered saline (PBS) were purchased from Thermo Fisher (Massachusetts, USA). Bovine serum albumin (BSA), Lactoferrin, Vitamin C, Vitamin B3 were purchased from FUJIFILM Wako Pure Chemical Corporation (Osaka, Japan). Biotin was purchased from Tokyo Chemical Industry Co., Ltd (Tokyo, Japan). Ultra-pure water was obtained from water purifier WL220 (Tokyo, Japan).

3D height graphing of the interdigital electrode and substrate was carried out by 3D laser microscopy OLS-4000. A 405 nm laser source is used. Raman measurements were carried out on a Nicolet Almega XR Raman spectroscope with a 532 nm laser. The Raman spectra of the

samples were acquired with a 100X objective, which reduced the spatial resolution to 1 μm. XPS measurements were performed on an AXIS-NOVA XPS system using an AlKα x-ray source. The incident and emission angles were 60 and 0° to the surface normal, respectively. The analyzer pass energies for the wide range and high-resolution measurements were set at 160 and 20 meV, respectively. The analyzer slit was set at 110 μm. A Keysight 4155B semiconductor parameter analyzer was used for the real-time GFET current measurements.

2.2. Device fabrication

The 4-inch 285 nm SiO_2/Si wafer was cut into the typical size of 1 cm × 1 cm by a dicing saw (DISCO Corporation, Japan). Each 1 cm × 1 cm cut SiO_2/Si was used as platform on which the interdigital electrode was fabricated. The interdigital shadow mask was carefully placed on the SiO_2/Si surface. Metal chromium (Cr)/gold (Au) was used as the deposition material. The metal deposition with desired thickness was performed by the electron beam vacuum evaporation deposition (EIKO Engineering, Japan) technique. The thickness of the deposited Cr/Au was about 50 nm/50 nm.

In the transfer process, the graphene on the copper foil was coated with a thin layer of PMMA using a spin coater (Mikasa Corporation, Japan) followed by 5 min of heating at 90 °C to evaporate the acetone solvent. The PMMA/graphene on the copper foil was cut into small pieces of 5 mm × 5 mm to suit the interdigital electrodes. Subsequent etching of the copper foil using ammonium peroxodisulfate aqueous solution left the PMMA/graphene film floating in the solution. After complete etching of copper foil, the PMMA/graphene film was transferred on the ultra-pure water, held for 30 min, then carefully transferred onto the surface of the interdigitated electrode substrate. The transferred PMMA/graphene film was then dried in air for 30 min at room temperature and heated at 60 °C for 30 min. Finally, the removal of PMMA with boiling acetone and isopropyl alcohol (IPA) left the graphene attached to the interdigital electrodes (Fei et al., 2017; Lin et al., 2012). The cleanliness of the transferred graphene was confirmed by optical images (Fig. S1 in supporting information, SI). Note that single and bilayer graphene transferred on SiO_2 substrate can be clearly visualized by optical microscope. There might have some undetected small patches of PMMA on the graphene, which we think does not invalidate the principle of the present GFET biosensing platform utilizing the avidin-biotin technology.

2.3. Graphene modification

Initially, the transferred graphene on interdigital electrodes was modified with PBASE, which is used as the linker for the non-covalent binding of the biomolecule with graphene. The surface modification with PBASE is very significant in maximizing device performances. Hence to find the best modification condition, the surface modification with PBASE was optimized by incubating the graphene on different interdigital electrodes samples in a dry dimethylformamide (DMF) solution of 50 mM PBASE for 1, 2, 4, 6 and 8 h at room temperature individually. The PBASE modified graphene was washed with methanol three times and dried with rotary pump. Then a pre-designed liquid pool made with silicone sheet was fixed on the top of the PBASE modified graphene so that the bio-solution to be tested can be injected into this test pool.

To capture the avidin molecules on the surface of PBASE modified graphene, 100 μl of 1 mg/ml avidin-PBS solution is injected into the pool, and held for 1 h at room temperature. Then the device is washed with 100 μl PBS three times. To prevent the non-specific binding of the residual surface regions (regions unmodified by PBASE) to other molecules, which may affect the signal during actual testing of the device, the remaining unmodified surface regions of the graphene were blocked by injecting 100 μl of 0.01 mg/ml BSA-PBS solution into the pool and holding for 1 h at room temperature followed by washing with 100 μl PBS three times.

2.4. Detection of biotin

Biotin buffer solutions with different concentrations were injected into the liquid pool while the real time current was measured to achieve the quantitative detection of biotin in PBS solution at pH 7.4. The source-drain voltage was maintained at 0.1 V while the gate (Si/SiO_2) was grounded. The Keysight 4155B semiconductor parameter analyzer was used in the real-time current measurements. The specificity of the graphene biosensor was investigated by two sets of experiments. In the first set, the same amount of PBS, BSA, biotin, BSA solutions were injected into the liquid pool separately while the current was monitored. Similarly, the same amount of Vitamin C, Vitamin B3, and lactoferrin were injected separately while monitoring the current.

3. Results and discussion

3.1. Characterization of interdigital electrodes

Fig. 1a shows optical images of the interdigital electrodes fabricated on SiO_2/Si substrate. The six pairs of the interdigital electrodes were fabricated on the 1 cm × 1 cm SiO_2/Si substrate. Electrode width was estimated to be 200 μm on average and the gap between the adjacent electrodes was 200 μm on average. From the 3D height profile, as shown in Fig. 1b, the thickness of the Cr/Au electrode was estimated to be about 100 nm.

3.2. Graphene transfer and modification

Fig. 2a shows the schematic of the top and side views of the transferred graphene on the interdigital electrodes (i.e. GFET). To ensure the quality of the transferred graphene, Raman measurements were done randomly over the entire regions. A typical Raman spectrum of the transferred graphene is shown in Fig. 2b. The two major peaks 2D and G characteristics of the clean graphene were observed. The absence of any defect induced peak around 1300 cm^{-1} (D band) indicates the cleanliness of the transferred graphene. The intensity ratio (I(2D)/I(G)) is 2.7, which is consistent with the intensity ratio of defect free monolayer graphene (Zhou et al., 2013). In addition, the 2D band of the bare graphene can be fitted into only one Lorentzian peak (R^2 is above 0.99) with the full width at half-maximum (FWHM) 30.8 cm^{-1} (Fig. S2 in SI), which also indicates the monolayer graphene (Hao et al., 2010).

The modification of graphene with the linker is an important part of designing a functional GFET biosensor system, because it realizes the immobilization of a receptor biomolecule (i.e., avidin) on the graphene which can specifically bind to a target ligand molecule (i.e., biotin). The modification steps are shown in Fig. 3. A conventional non-covalent linker used in the case of graphene, and the carbon nanotube-based device is PBASE, which is normally used to handle molecules containing lysine residue (Chen et al., 2001). The van der Waals force between the graphene and the pyrene backbone of PBASE molecule ensure their tight binding, this binding is also called π stacking. To the best of our knowledge, in spite of its importance, no detailed study on the coverage dependent modification and its effect on graphene's properties has been reported. Hence, to optimize the parameters for optimum coverage, we performed the time-dependent measurements. Fig. 4a shows the Raman spectra of transferred graphene after modification with PBASE for the different times indicated (1 h, 2 h, 4 h, 6 h, and 8 h). We can see that defect induced D (1350 cm^{-1}) and D′ band (1620 cm^{-1}) appear and the intensities of both bands increase with modification time. The D band is related to the disorder in the honeycomb structure of sp^2-hybridized carbon and arises from double resonances involving the nearest neighbour sites. The mechanism that gives rise to the D′ band is similar to that of the D band. Since the PBASE molecule is expected to be immobilized onto the graphene through non-covalent interaction, it is unlikely that

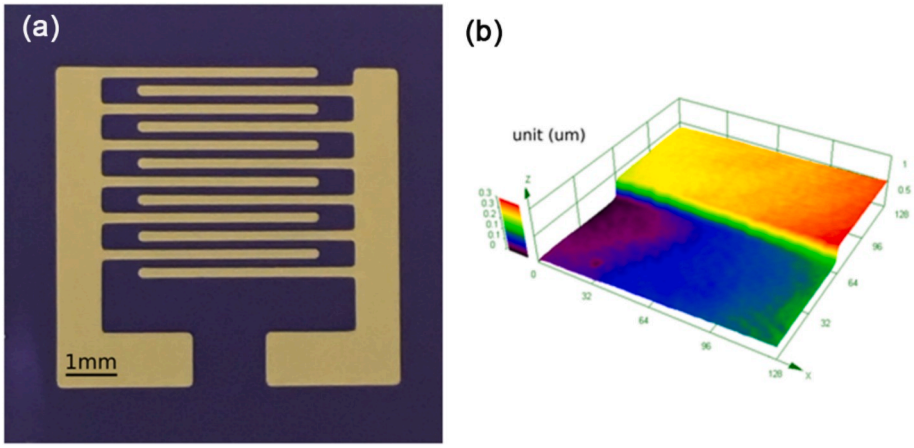

Fig. 1. (a) The full-scale optical image of the interdigital electrodes fabricated on a SiO_2/Si substrate. (b) The 3D image showing the height of the interdigital electrode and substrate.

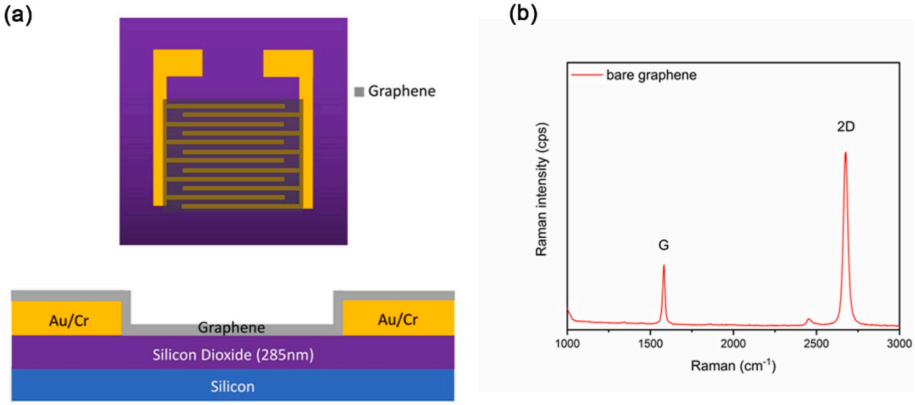

Fig. 2. (a) Schematic illustration of the graphene biosensor fabricated on SiO_2/Si substrate. Graphene was carefully transferred to cover all six pairs of interdigital electrodes. (b) The typical Raman spectrum of the graphene transferred onto the interdigital electrodes.

the defects in graphene arise from sp^3 carbons in the graphene's structure. The most likely reason for the appearance of the D and D′ bands is that the localized vibrational modes of the PBASE interact with the extended phonon modes of graphene. These results suggest that the degree of disorder of the sp^2 hybridized carbon system gradually increases as the modification time increases. Fig. 4b shows the ratios of 2D and G bands (2D/G) at different modification times. The 2D/G ratio gradually decreases and approaches 1 at around the modification time of 4 h. At 6 h, the 2D/G ratio still remains close to the value of 4 h but it further decreases at 8 h. Ratio of 1 is equivalent to that of the bilayer graphene. This indicates that the aggregation of pyrenyl groups onto the monolayer graphene forms a structure similar to that of bilayer graphene. Hence, to avoid any uncovered regions and excessive defects, the 4 h modification time seems optimal given the use of the 50 mM PBASE solution in dry dimethylformamide (DMF).

The modification of graphene with PBASE was also characterized by I–V and XPS measurements. Typical I–V curves for clean and PBASE modified (modified for 4 h) graphene are shown in Fig. 4c. A large shift of the Dirac point towards higher voltages is observed. This shifts in Dirac point indicates that the PBASE modification gives the graphene P-doping characteristics. The XPS spectrum shown in Fig. 4d shows a small N 1s peak around 400 eV following the PBASE modification, which ensures the presence of PBASE molecules on the graphene surface. Avidin is immobilized on the PBASE modified graphene through the interaction between lysine residue of avidin and N-hydroxysuccinimide ester group of PBASE. After avidin modification, a strong N 1s peak is observed, which indicates the increased number of nitrogen atoms from the avidin protein on the surface. No significant difference in the survey and C 1s spectra acquired before and after the PBASE modification of the bare graphene is observed (Figs. S3 and S4 in SI), which is in agreement with previous reports (Zhou et al., 2017). Thus the Raman, XPS and I–V measurements ensure the perfect PBASE modification of the graphene and immobilization of avidin onto the graphene channel of the GFET device.

3.3. Quantitative detection of biotin

Quantitative detection of biotin was performed by adding the biotin solutions to the test pool as shown in Fig. 5a. The 2-terminal measurement system is used while the gate-terminal was grounded. A blank test was run using 20 μl of PBS solution. Then 20 μl of each of the different concentrations of biotin-PBS solutions (180 fg/ml, 18 pg/ml, 1.8 ng/ml, 18 ng/ml, 36 ng/ml) were introduced to the test pool subsequently. No leakage of any liquid from the pool was observed during the analysis. Note that the concentration of the biotin solution in the test pool is lower than the original concentration because of the subsequent addition of the solution. Hence the actual concentrations of the test solutions are estimated to 90 fg/ml, 6.06 pg/ml, 0.45 ng/ml, 3.96 ng/ml, 9.33 ng/ml. Fig. 5b shows the Ids values while adding different concentrations of the biotin solutions in the real-time measurements. It is observed that as the concentration of biotin solution increases, the stable current value Ids gradually decreases. After the standard solution is added, the current Ids value stabilizes within 1 min. By monitoring the sharp current drops upon addition of the biotin-PBS solution and subsequent recovery to

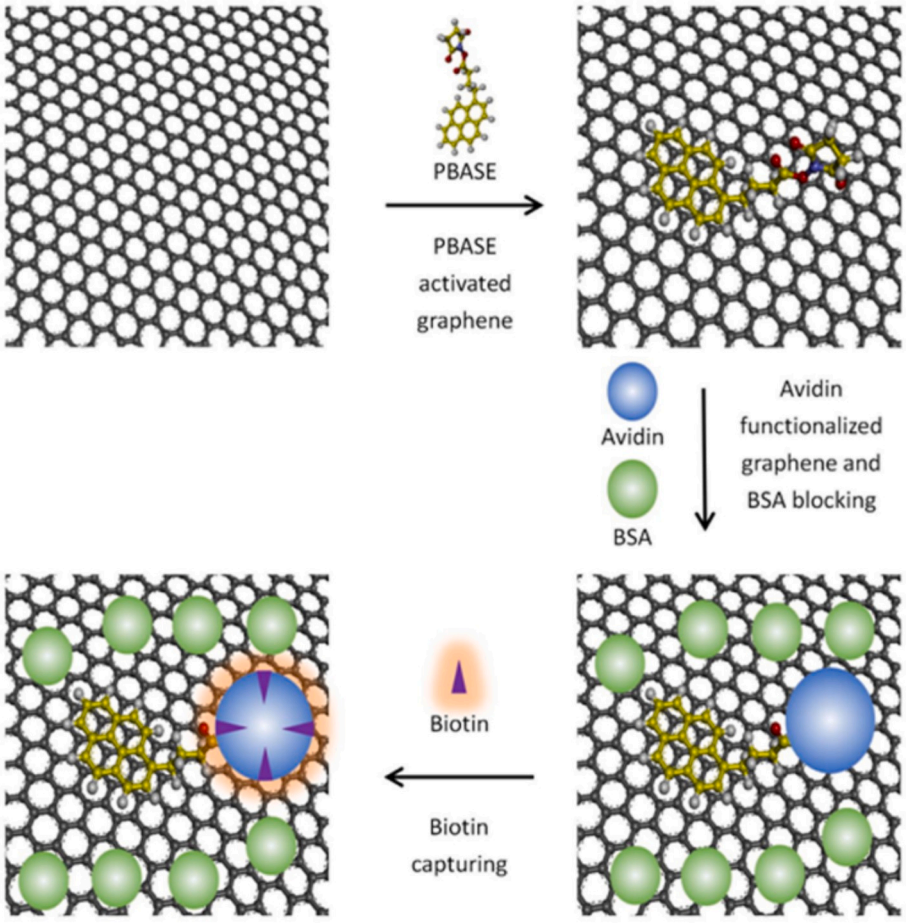

Fig. 3. The schematic illustration of the stepwise modification of graphene with avidin molecules followed by the binding of biotin molecules.

stable Ids, the biotin is detected down to the concentration level of 90 fg/ml. Detection of biotin with such ultra-sensitivity is achieved because of the extremely high conductivity of the graphene. The Ids current approaches the minimum value when the concentration of the biotin is close to 3.96 ng/ml. These results indicate that the present GFET biosensor can detect biotin levels as low as 90 fg/ml. When the concentration of the biotin is higher than 3.96 ng/ml, the graphene biosensor capability approaches saturated adsorption, i.e., the detection range of the present graphene biosensor is between 90 fg/ml and 3.96 ng/ml. Real-time Ids measurements were also performed using the biotin concentrations below the detection limit (i.e., 0.18 fg/ml, 1.8 fg/ml, 18 fg/ml), but no traceable change in stable Ids values were observed (Fig. S5 in SI). Note that reproducibility of biotin detection was confirmed in at least five independent measurements.

3.4. Estimation of dissociation constant of avidin-biotin interaction

Based on the real-time current change upon addition of the different concentrations of biotin solutions in PBS as shown in Fig. 5b, ΔI_{max} (maximum current change) and K_d (the dissociation constant) can be estimated using the Langmuir adsorption model $\Delta I = (C^*\Delta I_{max})/(C + K_d)$, C represents the concentration of the biotin. By fitting the experimental results shown in Fig. 5c, ΔI_{max} and K_d are estimated to -209 μA and 1.6×10^{-11} M, respectively. The correlation coefficient (R^2) is above 0.99. This Langmuir adsorption model has the potential to be used as the calibration curve for the quantitative detection of biotin in a given sample. Note that the theoretical dissociation constant of the avidin-biotin interaction is $\sim 1 \times 10^{-15}$ M (Gitlin et al., 1987). This difference in Kd value, which is in agreement with previous reports, is thought to be caused by binding of the avidin to the substrate surface (Neish et al., 2002; Nguyen et al., 2012; Wayment and Harris, 2009). In addition, the affinity of avidin for biotin may also have been affected when avidin is combined with PBASE.

3.5. The specificity of detection

In real applications, the sample to be tested contains not only the target molecule but also other molecules. Therefore, it is necessary to investigate sensor specificity. To confirm the specificity of the present GFET sensor, real time measurements with both the controlled and real samples were done. In the first set of controlled measurement, 20 μl of PBS, BSA, biotin, BSA solutions was poured sequentially into the test pool and observed the change in current. The concentrations of the BSA and biotin solutions were 0.01 mg/ml and 180 fg/ml, respectively. The results are shown in Fig. 5d. When the PBS and BSA solutions were added to the pool, the current signal remained almost unchanged, but upon addition of biotin solution, the current signal is dropped and remained unchanged even after introducing the BSA solution in the final step. In the second set of the experiment, 20 μl of 0.01 mg/ml of vitamin C, vitamin B3, and lactoferrin solutions in PBS was poured into the test pool sequentially and change in current was observed. The results are shown in Fig. S6 in SI. The results suggest that the current signal remains almost unchanged before and after the addition of the solution. These results indicate that the immobilized avidin does not interact with PBS, BSA, vitamin C, vitamin B3 and lactoferrin but readily interacted with biotin, i.e., the present GFET is very specific to the biotin molecules. For testing the specificity with a real sample, a preliminary experiment with chicken egg whites and yolk was performed (egg was purchased from

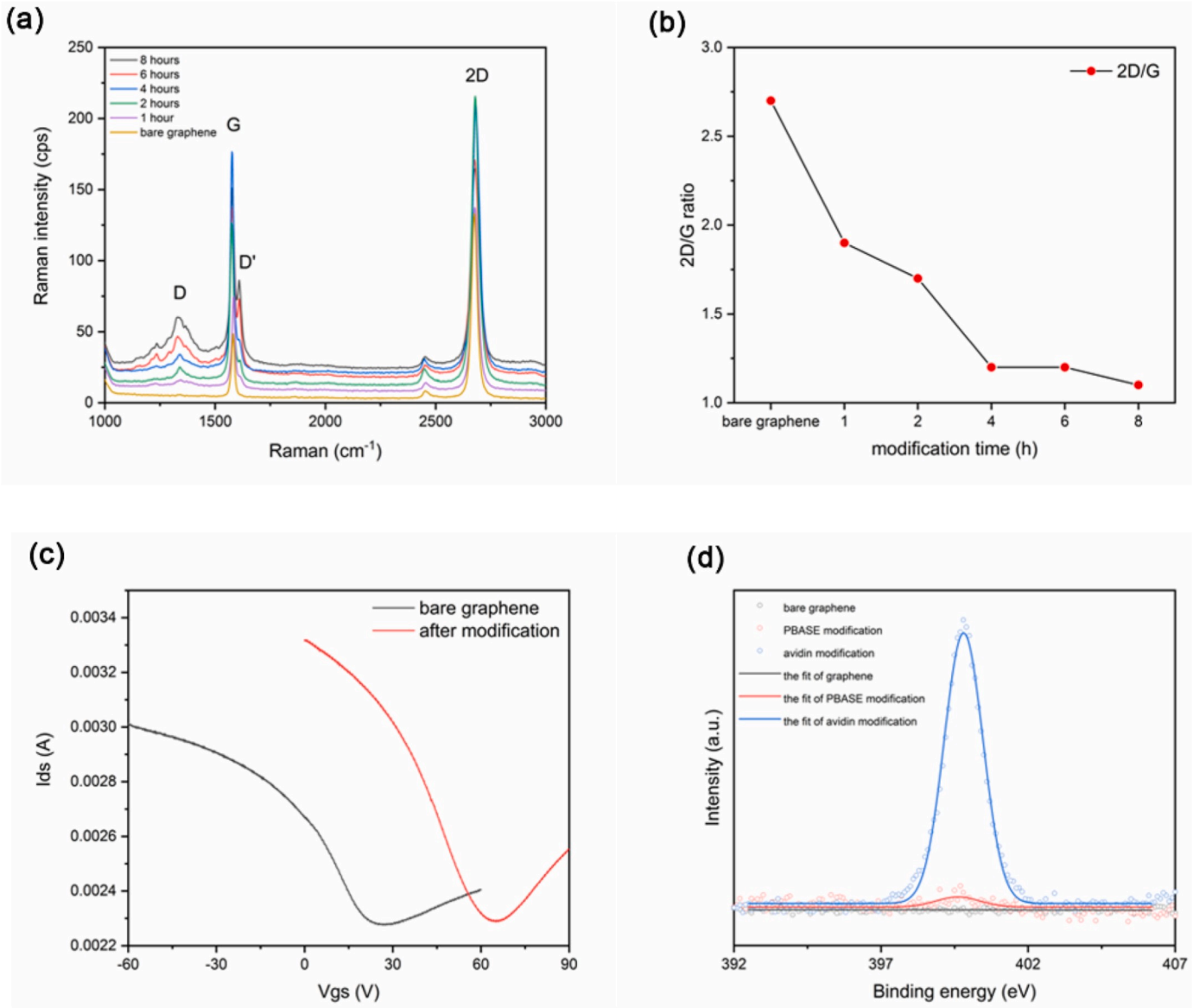

Fig. 4. (a) Raman spectra of the transferred graphene after modification with PBASE for the different times indicated (1 h, 2 h, 4 h, 6 h, 8 h). (b) The change of 2D/G ratio of the Raman spectra shown in (a). (c) The I–V curves of the bare graphene and after 4 h modification with PBASE. (d) The high-resolution N 1s XPS spectra of the clean, PBASE modified and avidin modified graphene.

supermarket). As expected, injection of 50 μl of egg yolk solution in PBS into the test pool of GFET induces the large drop of stable Ids current in real time measurements, which indicates the presence of free biotin or biotinylated compound. In contrast, injection of egg white solution in PBS does not induce any significant change in stable Ids current, which implies that no chemical components of egg white can non-specifically bind to the immobilized avidin on GFET. It is well known that the chicken egg yolk contains significant amount of biotin (13–25 μg/yolk), which is normally conjugated with specific biotin binding protein (BBP) (Meslar et al., 1978). These observations further support the specificity and sensing ability of the present GFET sensor in the case of a real sample. The detailed results are shown Fig. S7 in SI.

3.6. Exogenous biotin interferences

One of the main disadvantages of the avidin-biotin technology is the interference of exogenous biotin present in the blood of the subject which can range from 0.12 to 0.36 nM (Zempleni et al., 2009; Colon and Greene, 2018; Luong et al., 2019). Since the sensitivity of the present GFET lies in the pM range, the lowering or removal of biotin content in the target sample should be considered before charging the sample in the test pool. Different methods have been suggested for lowering or pre-removing the biotin from the blood sample. For example, biotin can be removed from blood samples by interacting the sample with avidin/streptavidin immobilized on insoluble matrices such as magnetic particles, polymers (e.g. agarose beads), silica, etc (Colon and Greene, 2018). Because of the short life time of biotin (2 h), the biotin content of the blood sample should be cleared within 4–5 h (Luong et al., 2019). Hence, for the analysis of blood sample using the present GFET sensor, the pre-removal of biotin content or the pre-estimation of the exogenous biotin interference should be considered. If the target sample is other than blood such as swab or exhaust gas, then the pre-removal of biotin will not be needed.

3.7. Comparative sensitivity and practical applicability

Recently, a number of studies have reported the utilization of avidin-biotin interaction focusing on sensing technology (Lin et al., 2019; Buzid

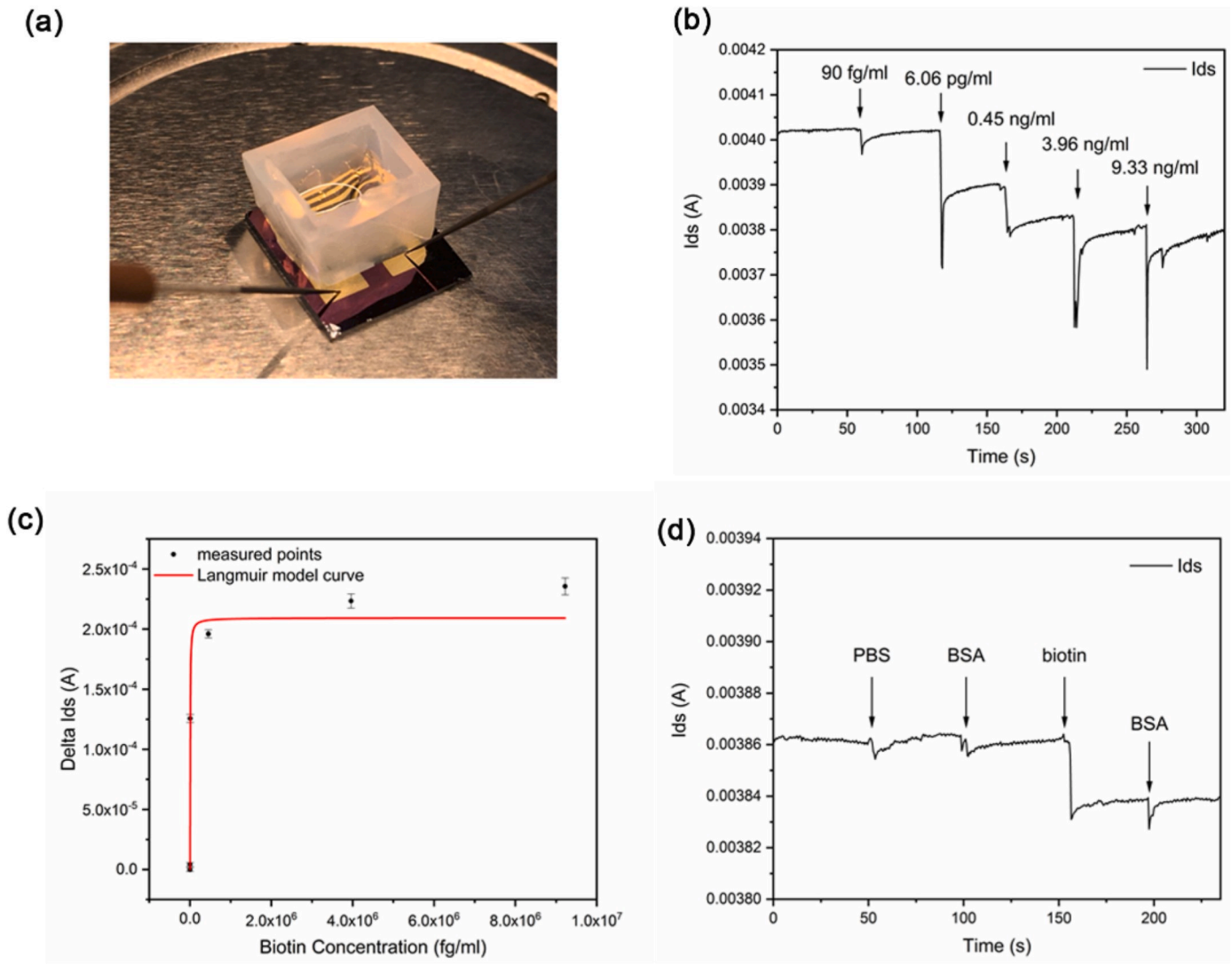

Fig. 5. (a) The 2-terminal real-time test system. A silicone pool is constructed onto the graphene transferred on interdigital electrodes fabricated on SiO_2/Si substrate. (b) The real time current (Ids) upon addition of different concentrations of biotin molecules. (c) Langmuir fitting to the changes of Ids at different concentration of biotin. (d) The real-time current (Ids) upon the addition of PBS, BSA, biotin, and BSA at different times.

et al., 2018, 2019; Kergaravat et al., 2012; Ho and Hung, 2008). The reported detection limits ranged from 2 pM to 84 nM using various detection methods such as competitive immunoassay, electrochemical, cyclic voltammetry and immunoaffinity chromatography as tabulated in Table 1. The GFET biosensor presented here shows the highest sensitivity and the minimum time requirement for real time detection.

Similar to the biotin-avidin system used in the conventional ELISA kits (Carinelli et al., 2016; Safaei et al., 2015; Tauriello et al., 2018), the present GFET biosensor can be utilized for detection of antigen-antibody, hormone-receptor, nucleic acid system in body fluid, tissue and cell, and other bioactive macromolecules through the judicious choice of biotinylation. Because of its small size, biotin conjugation with protein, nucleic acid and other macromolecules does not appear to change the original bioactivity of these molecules (Wilchek and Bayer, 1990). The widely used biotinylation methods utilize enzymatic biotinylation, primary amine biotinylation, sulfhydryl biotinylation, carboxyl biotinylation, glycoprotein biotinylation, and oligonucleotide biotinylation (Diamandis and Christopoulos, 1991). In the clinical detection applications, it can be used for the detection of biomarkers via anti-biotin antibodies or avidins/streptavidin-tagged detection strategies such as enzyme reporters (e.g., horseradish peroxidase, alkaline phosphatase) or fluorescent probes. For example, by monitoring the real time Ids of GFET upon the addition of biotinyled M1 protein (the universal biomarker for influenza virus) on the avidin or

Table 1
A comparison detection limits as regards biotin concentrations taken from recent publications.

Platform	Material	Method	Limit of detection	Time	Reference
Beads and gold nanoparticles	anti-biotin antibody	competitive immunoassay	2pM	15min	Lin et al. (2019)
Boron-doped diamond electrode	captavidin	electrochemical sensing	1 nM	10min	Buzid et al. (2019)
Boron-doped diamond electrode	streptavidin	electrochemical sensing	5 nM	10min	Buzid et al. (2018)
Electrochemical magneto biosensor	streptavidin	cyclic voltammetry	84 nM	40min	Kergaravat et al. (2012)
Sepharose beads	Anti-biotin antibody	immunoaffinity chromatographic	41pM	30min	(Ho and Hung, 2008)
Graphene FET biosensor	streptavidin (neutravidin)	current Ids real-time monitor	0.37 pM	1min	This work

streptavidin immobilized graphene channel, influenza can be diagnosed with ultrahigh sensitivity even before any symptom appears. Thus, because of the wide scope of avidin-biotin system, the present GFET is expected to be a breakthrough in the development of various ultrasensitive GFET biosensors for rapid and point-of-care low cost medical diagnosis. In addition, the ultra-high sensitivity of the present GFET is expected to allow quantitative detection of the exogenous biotin level in blood serum.

4. Conclusions

By combining the extreme electrical conductivity of graphene with the unique interaction between avidin and biotin molecules, we have realized a novel two terminal GFET biosensor for the detection of biotin with ultrahigh sensitivity and specificity. The GFET consists of six pairs of Cr/Au electrodes and an avidin immobilized single layer graphene channel supported on the Si/SiO_2 substrate. By monitoring the source-drain current change upon addition of biotin solution in BSA, biotin can be detected to levels as low as 90 fg/ml (0.37 pM), and so is the most sensitive GFET for biomolecule detection. The detection range of the present GFET biosensor is estimated to lie between 90 fg/ml and 3.96 ng/ml. The high specificity of the GFET was confirmed both by controlled and real samples. Based on the Langmuir adsorption model, ΔI_{max} and K_d are estimated to be -209 μA and 1.6×10^{-11} M. The correlation coefficient (R^2) is about 0.99. Because of the wide range of conjugation capability of biotin molecules through biotinylation, the present GFET can be employed for the detection of various biomarkers and bio-macromolecules. In addition, it may also be used for the rapid quantitative detection of exogenous biotin. Because of its real-time rapid detection, ultra-low detection limit, and high specificity, the present GFET biosensor is expected to be a breakthrough in medical devices offering real-time point-of-care clinical diagnosis.

Declaration of competing interest

The authors declare that they have no known competing financial interests or personal relationships that could have appeared to influence the work reported in this paper.

CRediT authorship contribution statement

Shiyu Wang: Conceptualization, Writing - original draft, Methodology. **Md Zakir Hossain:** Conceptualization, Writing - review & editing. **Kazuo Shinozuka:** Supervision. **Natsuhiko Shimizu:** Methodology. **Shunya Kitada:** Methodology. **Takaaki Suzuki:** Supervision. **Ryo Ichige:** Supervision. **Anna Kuwana:** Supervision. **Haruo Kobayashi:** Conceptualization, Funding acquisition, Supervision, Writing - review & editing.

Acknowledgement

This work was conducted at Nano-Processing Facility, National Institute of Advanced Industrial Science and Technology (AIST), Japan. Thanks are due to Professor Hayato Sone, Professor Kenta Miura for guiding the equipment operation, as well as Professor Noriyuki Koibuchi for his helpful comments and suggestions.

Appendix A. Supplementary data

Supplementary data to this article can be found online at https://doi.org/10.1016/j.bios.2020.112363.

References

Afsahi, S., Lerner, M.B., Goldstein, J.M., Lee, J., Tang, X., Bagarozzi, D.A., Pan, D., Locascio, L., Walker, A., Barron, F., Goldsmith, B.R., 2018. Novel graphene-based biosensor for early detection of Zika virus infection. Biosens. Bioelectron. 100, 85–88. https://doi.org/10.1016/j.bios.2017.08.051.

Alberto, A., Pier, L.S., 2020. Trends in the change in graphene conductivity upon gas adsorption: the relevance of orbital distortion. J. Phys. Chem. Lett. 11, 2737–2741. https://doi.org/10.1021/acs.jpclett.0c00379.

Agnolon, V., Contato, A., Meneghello, A., Tagliabue, E., Toffoli, G., Gion, M., Polo, F., Fabricio, A.S.C., 2020. ELISA assay employing epitope-specific monoclonal antibodies to quantify circulating HER2 with potential application in monitoring cancer patients undergoing therapy with trastuzumab. Sci. Rep. 10, 1–12. https://doi.org/10.1038/s41598-020-59630-y.

Ballesta-Claver, J., Ametis-Cabello, J., Morales-Sanfrutos, J., Megía-Fernández, A., Valencia-Mirón, M.C., Santoyo-González, F., Capitán-Vallvey, L.F., 2012. Electrochemiluminescent disposable cholesterol biosensor based on avidin–biotin assembling with the electroformed luminescent conducting polymer poly(luminol-biotinylated pyrrole). Anal. Chim. Acta 754, 91–98. https://doi.org/10.1016/j.aca.2012.10.006.

Ben Aissa, A., Herrera-Chacon, A., Pupin, R.R., Sotomayor, M.D.P.T., Pividori, M.I., 2017. Magnetic molecularly imprinted polymer for the isolation and detection of biotin and biotinylated biomolecules. Biosens. Bioelectr., Spec. Issue Sel. Pap. 26th Anniv. World Congr. Biosens. (Part I) 88, 101–108. https://doi.org/10.1016/j.bios.2016.07.096.

Buzid, A., Hayes, P.E., Glennon, J.D., Luong, J.H.T., 2019. Captavidin as a regenerable biorecognition element on boron-doped diamond for biotin sensing. Anal. Chim. Acta 1059, 42–48. https://doi.org/10.1016/j.aca.2019.01.058.

Buzid, A., McGlacken, G.P., Glennon, J.D., Luong, J.H.T., 2018. Electrochemical sensing of biotin using nafion-modified boron-doped diamond electrode. ACS Omega 3, 7776–7782. https://doi.org/10.1021/acsomega.8b01209.

Cai, B., Huang, L., Zhang, H., Sun, Z., Zhang, Z., Zhang, G.-J., 2015. Gold nanoparticles-decorated graphene field-effect transistor biosensor for femtomolar MicroRNA detection. Biosens. Bioelectron. 74, 329–334. https://doi.org/10.1016/j.bios.2015.06.068.

Carinelli, S., Xufré, C., Alegret, S., Martí, M., Pividori, M.I., 2016. CD4 quantification based on magneto ELISA for AIDS diagnosis in low resource settings. Talanta 160, 36–45. https://doi.org/10.1016/j.talanta.2016.06.055.

Chen, R.J., Zhang, Y., Wang, D., Dai, H., 2001. Noncovalent sidewall functionalization of single-walled carbon nanotubes for protein immobilization. J. Am. Chem. Soc. 123, 3838–3839. https://doi.org/10.1021/ja010172b.

Chivers, C.E., Koner, A.L., Lowe, E.D., Howarth, M., 2011. How the biotin–streptavidin interaction was made even stronger: investigation via crystallography and a chimaeric tetramer. Biochem. J. 435, 55–63. https://doi.org/10.1042/BJ20101593.

Colon, P.J., Greene, D.N., 2018. Biotin interference in clinical immunoassays. J. Appl. Lab Med. 2, 941–951. https://doi.org/10.1373/jalm.2017.024257.

Diamandis, E.P., Christopoulos, T.K., 1991. The biotin-(strept)avidin system: principles and applications in biotechnology. Clin. Chem. 37, 625–636. https://doi.org/10.1093/clinchem/37.5.625.

Deana, K.H.T., Tyler, J.L., Clare, W., Iain, E.D., Sami, R., Armando E, del R.H., Norbert, K., 2019. Chemically functionalized graphene FET biosensor for the label-free sensing of exosomes. Sci. Rep. 9, 13946 https://doi.org/10.1038/s41598-019-50412-9.

Fiala, C., Diamandis, E.P., 2018. Utility of circulating tumor DNA in cancer diagnostics with emphasis on early detection. BMC Med. 16, 166. https://doi.org/10.1186/s12916-018-1157-9.

Fei, H., Shaochuan, C., Xianhu, L., Bin, Y., Xu, J., Yuanyuan, S., Mario, L., 2017. Graphene coated nanoprobes: a review. Crystals 269 (9), 7. https://doi.org/10.3390/cryst7090269.

Frank, S., 2010. Graphene transistors. Nat. Nanotechnol. 5, 487–496. https://doi.org/10.1038/nnano.2010.89.

Geim, A.K., Novoselov, K.S., 2009. The rise of graphene. In: Nanoscience and Technology. Co-Published with Macmillan Publishers Ltd, UK, pp. 11–19. https://doi.org/10.1142/9789814287005_0002.

Gitlin, G., Bayer, E.A., Wilchek, M., 1987. Studies on the biotin-binding site of avidin. Lysine residues involved in the active site. Biochem. J. 242, 923–926. https://doi.org/10.1042/bj2420923.

Green, N.M., 1963. Avidin. 1. The use of [14C]biotin for kinetic studies and for assay. Biochem. J. 89, 585–591.

Guesdon, J.L., Ternynck, T., Avrameas, S., 1979. The use of avidin-biotin interaction in immunoenzymatic techniques. J. Histochem. Cytochem. 27, 1131–1139. https://doi.org/10.1177/27.8.90074.

Gutiérrez-Zúñiga, G.G., Hernández-López, J.L., 2016. Sensitivity improvement of a sandwich-type ELISA immunosensor for the detection of different prostate-specific antigen isoforms in human serum using electrochemical impedance spectroscopy and an ordered and hierarchically organized interfacial supramolecular architecture. Anal. Chim. Acta 902, 97–106. https://doi.org/10.1016/j.aca.2015.10.042.

Hao, Y., Wang, Y., Wang, L., Ni, Z., Wang, Z., Wang, R., Koo, C.K., Shen, Z., Thong, J.T.L., 2010. Probing layer number and stacking order of few-layer graphene by Raman spectroscopy. Small 6, 195–200. https://doi.org/10.1002/smll.200901173.

Helppolainen, S.H., Nurminen, K.P., Määttä, J.A.E., Halling, K.K., Slotte, J.P., Huhtala, T., Liimatainen, T., Ylä-Herttuala, S., Airenne, K.J., Närvänen, A., Jänis, J., Vainiotalo, P., Valjakka, J., Kulomaa, M.S., Nordlund, H.R., 2007. Rhizavidin from Rhizobium etli: the first natural dimer in the avidin protein family. Biochem. J. 405, 397–405. https://doi.org/10.1042/BJ20070076.

Ho, J.A., Hung, C.-H., 2008. Using liposomal fluorescent biolabels to develop an immunoaffinity chromatographic biosensing system for biotin. Anal. Chem. 80, 6405–6409. https://doi.org/10.1021/ac800850w.

Hsu, S., Raine, L., Fanger, H., 1981. The use of antiavidin antibody and avidin-biotin-peroxidase complex in immunoperoxidase technics. Am. J. Clin. Pathol. 75, 816–821. https://doi.org/10.1093/ajcp/75.6.816.

Hsu, S.M., Raine, L., Fanger, H., 1981. Use of avidin-biotin-peroxidase complex (ABC) in immunoperoxidase techniques: a comparison between ABC and unlabeled antibody (PAP) procedures. J. Histochem. Cytochem. 29, 577–580. https://doi.org/10.1177/29.4.6166661.

Hu, G., Xu, C., Sun, Z., Wang, S., Cheng, H.-M., Li, F., Ren, W., 2016. 3D graphene-foam–reduced-graphene-oxide hybrid nested hierarchical networks for high-performance Li–S batteries. Adv. Mater. 28, 1603–1609. https://doi.org/10.1002/adma.201504765.

Kergaravat, S.V., Gómez, G.A., Fabiano, S.N., Laube Chávez, T.I., Pividori, M.I., Hernández, S.R., 2012. Biotin determination in food supplements by an electrochemical magneto biosensor. Talanta 97, 484–490. https://doi.org/10.1016/j.talanta.2012.05.003.

Lakshmipriya, T., Gopinath, S.C.B., Tang, T.-H., 2016. Biotin-streptavidin competition mediates sensitive detection of biomolecules in enzyme linked immunosorbent assay. PloS One 11. https://doi.org/10.1371/journal.pone.0151153.

Lin, W.-Z., Chen, Y.-H., Liang, C.-K., Liu, C.-C., Hou, S.-Y., 2019. A competitive immunoassay for biotin detection using magnetic beads and gold nanoparticle probes. Food Chem. 271, 440–444. https://doi.org/10.1016/j.foodchem.2018.07.152.

Lin, Y.-C., Lu, C.-C., Yeh, C.-H., Jin, C., Suenaga, K., Chiu, P.-W., 2012. Graphene annealing: how clean can it Be? Nano Lett. 12, 414–419. https://doi.org/10.1021/nl203733r.

Luong, J.H.T., Male, K.B., Glennon, J.D., 2019. Biotin interference in immunoassays based on biotin-strept(avidin) chemistry: an emerging threat. Biotechnol. Adv. 37, 634–641. https://doi.org/10.1016/j.biotechadv.2019.03.007.

Machado N, B, Serp, P, 2012. Graphene-based materials for catalysis. Catal. Sci. Technol. 2 (1), 54–75. https://doi.org/10.1039/C1CY00361E.

Matsumoto, K., 2015. Frontiers of Graphene and Carbon Nanotubes: Devices and Applications. Springer.

Meslar, H.W., Camper, S.A., White III, H.B., 1978. Biotin-binding protein from egg yolk. A protein distinct from egg white avidin. J. Biol. Chem. 253, 6979–6982. https://doi.org/10.1186/1472-6807-7-8.

Morag, E., Bayer, E.A., Wilchek, M., 1996. Reversibility of biotin-binding by selective modification of tyrosine in avidin. Biochem. J. 316, 193–199. https://doi.org/10.1042/bj3160193.

Neish, C.S., Martin, I.L., Henderson, R.M., Edwardson, J.M., 2002. Direct visualization of ligand-protein interactions using atomic force microscopy. Br. J. Pharmacol. 135, 1943–1950. https://doi.org/10.1038/sj.bjp.0704660.

Nguyen, T.T., Sly, K.L., Conboy, J.C., 2012. Comparison of the energetics of avidin, streptavidin, NeutrAvidin, and anti-biotin antibody binding to biotinylated lipid bilayer examined by second-harmonic generation. Anal. Chem. 84, 201–208. https://doi.org/10.1021/ac202375n.

Novoselov, K.S., Geim, A.K., Morozov, S.V., Jiang, D., Zhang, Y., Dubonos, S.V., Grigorieva, I.V., Firsov, A.A., 2004. Electric field effect in atomically thin carbon films. Science 306, 666–669. https://doi.org/10.1126/science.1102896.

Nozaki, R., Ikuta, T., Ueno, K., Tsukakoshi, K., Ikebukuro, K., Maehashi, K., 2020. Ethanol detection at the parts per billion level with single-stranded-DNA-modified graphene field-effect transistors. Phys. Status Solidi 257, 1900376. https://doi.org/10.1002/pssb.201900376.

Ohno, Y., Maehashi, K., Matsumoto, K., 2010. Label-free biosensors based on aptamer-modified graphene field-effect transistors. J. Am. Chem. Soc. 132, 18012–18013. https://doi.org/10.1021/ja108127r.

Ohno, Y., Maehashi, K., Yamashiro, Y., Matsumoto, K., 2009. Electrolyte-gated graphene field-effect transistors for detecting pH and protein adsorption. Nano Lett. 9, 3318–3322. https://doi.org/10.1021/nl901596m.

Pan, L.-H., Kuo, S.-H., Lin, T.-Y., Lin, C.-W., Fang, P.-Y., Yang, H.-W., 2017. An electrochemical biosensor to simultaneously detect VEGF and PSA for early prostate cancer diagnosis based on graphene oxide/ssDNA/PLLA nanoparticles. Biosens. Bioelectr., 2D Mater. Biosens. Bioelectr. 89, 598–605. https://doi.org/10.1016/j.bios.2016.01.077.

Rubio, E., Zboromyrska, Y., Pitart, C., Campo, I., Alejo-Cancho, I., Fasanella, A., Vergara, A., Marco, F., Vila, J., 2017. Evaluation of a rapid immunochromatographic test for the detection of OXA-48 carbapenemase. Diagn. Microbiol. Infect. Dis. 87, 266–267. https://doi.org/10.1016/j.diagmicrobio.2016.12.001.

Safaei, T.S., Mohamadi, R.M., Sargent, E.H., Kelley, S.O., 2015. In situ electrochemical ELISA for specific identification of captured cancer cells. ACS Appl. Mater. Interfaces 7, 14165–14169. https://doi.org/10.1021/acsami.5b02404.

Singh Raman, R.K., Chakraborty Banerjee, P., Lobo, D.E., Gullapalli, H., Sumandasa, M., Kumar, A., Choudhary, L., Tkacz, R., Ajayan, P.M., Majumder, M., 2012. Protecting copper from electrochemical degradation by graphene coating. Carbon 50, 4040–4045. https://doi.org/10.1016/j.carbon.2012.04.048.

Taniguchi, Y., Miki, T., Ohno, Y., Nagase, M., Arakawa, Y., Yasuzawa, M., 2019. Observation of the interaction between avidin and iminobiotin using a graphene FET on a SiC substrate. Jpn. J. Appl. Phys. 58, SDDD02. https://doi.org/10.7567/1347-4065/ab0544.

Tauriello, D.V.F., Palomo-Ponce, S., Stork, D., Berenguer-Llergo, A., Badia-Ramentol, J., Iglesias, M., Sevillano, M., Ibiza, S., Cañellas, A., Hernando-Momblona, X., Byrom, D., Matarin, J.A., Calon, A., Rivas, E.I., Nebreda, A.R., Riera, A., Attolini, C. S.-O., Batlle, E., 2018. TGFβ drives immune evasion in genetically reconstituted colon cancer metastasis. Nature 554, 538–543. https://doi.org/10.1038/nature25492.

Wang, Y, Wang, Y, Chen, Y, Qin, Q, 2020. Unique epidemiological and clinical features of the emerging 2019 novel coronavirus pneumonia (COVID-19) implicate special control measures. Journal of Medical Virology 92, 568–576. https://doi.org/10.1002/jmv.25748.

Wang, Z., Yi, K., Lin, Q., Yang, L., Chen, X., Chen, H., Liu, Y., Wei, D., 2019. Free radical sensors based on inner-cutting graphene field-effect transistors. Nat. Commun. 10, 1–10. https://doi.org/10.1038/s41467-019-09573-4.

Wayment, J.R., Harris, J.M., 2009. Biotin−Avidin binding kinetics measured by single-molecule imaging. Anal. Chem. 81, 336–342. https://doi.org/10.1021/ac801818t.

Wen, L., Li, F., Cheng, H.-M., 2016. Carbon nanotubes and graphene for flexible electrochemical energy storage: from materials to devices. Adv. Mater. 28, 4306–4337. https://doi.org/10.1002/adma.201504225.

Wilchek, M., Bayer, E.A., 1990. [2] Introduction to avidin-biotin technology. In: Wilchek, M., Bayer, E.A. (Eds.), Methods in Enzymology, Avidin-Biotin Technology. Academic Press, pp. 5–13. https://doi.org/10.1016/0076-6879(90)84256-G.

Wu, Z.-S., Zhou, G., Yin, L.-C., Ren, W., Li, F., Cheng, H.-M., 2012. Graphene/metal oxide composite electrode materials for energy storage. Nano Energy 1, 107–131. https://doi.org/10.1016/j.nanoen.2011.11.001.

Xiao, H., Wu, Z.-S., Chen, L., Zhou, F., Zheng, S., Ren, W., Cheng, H.-M., Bao, X., 2017. One-step device fabrication of phosphorene and graphene interdigital micro-supercapacitors with high energy density. ACS Nano 11, 7284–7292. https://doi.org/10.1021/acsnano.7b03288.

Xu, S., Zhan, J., Man, B., Jiang, S., Yue, W., Gao, S., Guo, C., Liu, H., Li, Z., Wang, J., Zhou, Y., 2017. Real-time reliable determination of binding kinetics of DNA hybridization using a multi-channel graphene biosensor. Nat. Commun. 8, 1–10. https://doi.org/10.1038/ncomms14902.

Yang, K., Feng, L., Shi, X., Liu, Z., 2012. Nano-graphene in biomedicine: theranostic applications. Chem. Soc. Rev. 42, 530–547. https://doi.org/10.1039/C2CS35342C.

Yang, X., Cheng, C., Wang, Y., Qiu, L., Li, D., 2013. Liquid-mediated dense integration of graphene materials for compact capacitive energy storage. Science 341, 534–537. https://doi.org/10.1126/science.1239089.

Yang, X., Yuan, R., Chai, Y., Zhuo, Y., Mao, L., Yuan, S., 2010. Ru(bpy)32+-doped silica nanoparticles labeling for a sandwich-type electrochemiluminescence immunosensor. Biosens. Bioelectron. 25, 1851–1855. https://doi.org/10.1016/j.bios.2009.12.027.

Yang, Y., Yang, X., Zou, X., Wu, S., Wan, D., Cao, A., Liao, L., Yuan, Q., Duan, X., 2017. Ultrafine graphene nanomesh with large on/off ratio for high-performance flexible biosensors. Adv. Funct. Mater. 27, 1604096 https://doi.org/10.1002/adfm.201604096.

Yang, Y.-C., Tseng, W.-L., 2016. 1,4-Benzenediboronic-Acid-Induced aggregation of gold nanoparticles: application to hydrogen peroxide detection and biotin–avidin-mediated immunoassay with naked-eye detection. Anal. Chem. 88, 5355–5362. https://doi.org/10.1021/acs.analchem.6b00668.

Yu, Y., Li, Y.-T., Jin, D., Yang, F., Wu, D., Xiao, M.-M., Zhang, H., Zhang, Z.-Y., Zhang, G.-J., 2019. Electrical and label-free quantification of exosomes with a reduced graphene oxide field effect transistor biosensor. Anal. Chem. 91, 10679–10686. https://doi.org/10.1021/acs.analchem.9b01950.

Zempleni, J., Wijeratne, S.S.K., Hassan, Y.I., 2009. Biotin. BioFactors 35, 36–46. https://doi.org/10.1002/biof.8.

Zhang, H., Cheng, H.-M., Ye, P., 2018. 2D nanomaterials: beyond graphene and transition metal dichalcogenides. Chem. Soc. Rev. 47, 6009–6012. https://doi.org/10.1039/C8CS90084A.

Zhou, H., Yu, W.J., Liu, L., Cheng, R., Chen, Y., Huang, X., Liu, Y., Wang, Y., Huang, Y., Duan, X., 2013. Chemical vapour deposition growth of large single crystals of monolayer and bilayer graphene. Nat. Commun. 4, 1–8. https://doi.org/10.1038/ncomms3096.

Zhou, L., Mao, H., Wu, C., Tang, L., Wu, Z., Sun, H., Zhang, H., Zhou, H., Jia, C., Jin, Q., Chen, X., Zhao, J., 2017. Label-free graphene biosensor targeting cancer molecules based on non-covalent modification. Biosens. Bioelectron. 87, 701–707. https://doi.org/10.1016/j.bios.2016.09.025.